



Transition from the displacement discontinuity limit to the resonant scattering regime for fracture interface waves

D.D. Nolte^{a,*}, L.J. Pyrak-Nolte^a, J. Beachy^b, C. Ziegler^b

^aDepartment of Physics, Purdue University, West Lafayette, IN 47907-1396, USA

^bDepartment of Civil Engineering and Geological Sciences, University of Notre Dame, Notre Dame, IN 46556-0767, USA

Accepted 7 October 1999

Abstract

The validity of the displacement discontinuity model for elastic wave propagation across and along fractures is related to the spacing of asperities in fractures. In this paper, the transition from the displacement-discontinuity regime to the resonant scattering of Rayleigh waves is explicitly observed for waves propagating along synthetic fractures. The fractures are engineered to have increasing asperity separation with fixed aperture orientation. The seismic signals of elastic interface waves for all three polarizations S_v , S_h and P propagating along the synthetic fractures are recorded, and the waveforms are analyzed using the new Nolte–Hilbert wavelet that balances time-frequency localization without violating the wavelet admissibility condition which impedes the use of the Morlet wavelet transform. The wavelet spectra of the elastic waves are measured in response to the changing asperity separation for waves propagating parallel and perpendicular to the asperities. Clear evidence for both Rayleigh-mode and P -mode fracture interface waves, as well as resonantly scattered Rayleigh waves, are observed in the wavelet transforms. © 2000 Elsevier Science Ltd. All rights reserved.

1. Introduction

Fractures in solid media represent mechanical discontinuities that strongly affect the propagation of elastic waves either across or along the fracture plane. Signatures of the fracture properties, especially fracture specific stiffness, appear in the amplitudes, phases and velocities of the elastic waves. These waves therefore become probes of the fracture, with potential benefits for predicting fracture mechanical stability and fluid flow through the fracture [22]. One of the physical models used to analyze the seismic properties of fractures is the displacement discontinuity model [16,17], also known as the linear slip interface model [12,26], or incomplete or imperfect interface model [23]. The displacement discontinuity model assumes that the stresses across a fracture are continuous but that the

displacements are not. The discontinuity in displacement is inversely proportional to the quantity called specific stiffness of the fracture.

Specific stiffness plays a purely phenomenological role in the displacement discontinuity model as a proportionality factor that relates the displacement discontinuity to the elastic stress of the propagating wave. However, there is considerable importance in connecting the fracture specific stiffness to the physical properties of the fracture, such as the geometry of the voids and asperities, because ultimately it is the geometry of the voids and asperities that determine the hydraulic–mechanical properties of interest for a fracture [4].

In the effort to connect stiffness with physical fracture properties, quasi-static stiffness of a fracture can be defined by relating far-field fracture displacement with the applied stress across a fracture. The specific stiffness of the fracture in this case depends on the number and distribution of the asperities (points of contact between the two fracture surfaces),

* Corresponding author. Fax: +1-765-494-0706.

E-mail address: nolte@physics.purdue.edu (D.D. Nolte).

[1,2,7,10,11]. Alternatively, in the displacement discontinuity model, dynamic stiffness can be viewed to be caused by finely distributed springs that couple the two half-spaces on either side of the fracture.

One of the outstanding problems in the study of fracture stiffness and its relation to fracture geometry is understanding the connection between quasi-static mechanical stiffness and the dynamic stiffness extracted from displacement discontinuity theory. Dynamic and quasi-static stiffnesses are not equal [16,18], with dynamic stiffness always exceeding the magnitude of quasi-static stiffness. Furthermore, even within the dynamic stiffness itself, there is often a frequency dependence in which the stiffness increases with increasing frequency [27]. The mechanisms for this frequency-dependent stiffness are not fully understood, although part of the frequency dependence may not be dynamical in nature, but would be a simple consequence of wavefront averaging over inhomogeneous distributions of local stiffnesses along a fracture [19].

This issue of inhomogeneous distributions of stiffnesses along a fracture interface raises many interesting questions about what seismic propagation experiments actually measure. For instance, the concept of finely distributed asperities, represented as springs coupling the two faces of a fracture, is expected to be valid only if the spacing between the asperities is much smaller than a wavelength. However, if the distribution of the asperities is strongly inhomogeneous, then even if the individual asperity separations satisfy this condition, the correlation length describing the fluctuations in the stiffnesses may be much larger than the average asperity spacing. In addition, short pulses of seismic energy are broad-band waves that contain a spectrum of wavelengths, some of which may be longer than the correlation length, but others may not. This situation would lead to complicated behavior as low frequencies probe large areas of asperities and high frequencies probe smaller areas of asperities, and are therefore each subject to different average values. Added to this complexity is the possibility for resonant scattering when the fluctuation lengths become comparable to a wavelength, perhaps calling into question the validity of the displacement discontinuity theory. For instance, periodic asperity spacings that are on the order of a wavelength can produce resonant (Bragg) reflections that show up clearly in time-frequency (wavelet) analyses of the received waveforms.

In this paper, we study the physical validity of the displacement discontinuity model as it relates to the question of asperity spacing, and we explicitly observe the transition from the displacement discontinuity limit to the resonant scattering regime. We study the seismic response of elastic interface waves for all three polarizations (S_v , S_h and P-waves) propagating along synthetic fractures. The fractures are engineered to give

increasing asperity separation, and we monitor the spectral response of the elastic waves to the changing separation. We first describe the physical properties of fracture interface waves into which energy from S_v and P-waves are partitioned, then describe the experimental set-up for studying the effect of asperity spacing on these interface waves. The waveforms are analyzed using the Nolte–Hilbert wavelet that balances the time-bandwidth product for time-frequency analysis without violating the admissibility condition that has previously impeded the use of the Morlet wavelet transform. Clear evidence for both fracture interface waves as well as resonantly scattered Rayleigh waves is observed in the wavelet transforms, and the wavelet transforms are used to extract the fracture wave dispersion. The paper finishes by revisiting the conditions for validity of the displacement discontinuity model in view of the new results presented here.

2. Fracture interface waves

Fracture interface waves have been demonstrated to propagate along natural and synthetic fractures at the laboratory scale [5,6,14,20,24,25]. Fracture interface waves can be viewed as coupled Rayleigh waves in which Rayleigh waves travel along each surface of the fracture and are coupled through the points of contact between the two surfaces. The analytic and numerical solutions have shown that this coupling produces two dispersive waves that exhibit both longitudinal and transverse particle motions, and have a velocity that ranges between the bulk shear wave velocity and the Rayleigh wave velocity [9,17].

In addition to the Rayleigh-mode interface waves, numerical [8] and experimental [6,25,28] evidence has accumulated supporting the existence of a P-mode interface wave that arrives coincident with the bulk P-wave, but with a distinct phase and different frequency content. This wave has both transverse and longitudinal displacements, similar to the Rayleigh-mode interface wave, and has been shown to be sensitive to fracture properties, such as stiffness [25,28]. These waves were also used to monitor precursors to failure during fracturing [25].

The sensitivity of both the Rayleigh-mode and P-mode interface waves to fracture stiffness makes them candidates as remote probes for testing fracture properties. Furthermore, their sensitivity to fracture stiffness makes them ideal probes to test the limits of validity of the displacement discontinuity model. The manner in which these waves evolve as the asperity spacing increases will help illustrate the different regimes of propagation, including resonant scattering. These effects can be compared against the propagation of S_h waves as a control case because the S_h waves

Table 1

The lead strip width, the gap between strips, the number of strips per sample, and the contact area for each synthetic fracture

Synthetic fracture ^a	Strip width (mm)	Gap between strips (mm)	Number of strips	Contact area (%)
1 × 1	1	1	145	50
2 × 2	2	2	73	50
4 × 4	4	4	36	50
8 × 8	8	8	18	50

^a For each synthetic fracture the strip thickness was 25 microns and the strip length was 0.29 m.

produce no elastic interface wave. It is, in particular, the comparison between the S_h and P-wave cases that lends further support in favor of a distinct P-mode interface wave.

3. Experimental set-up

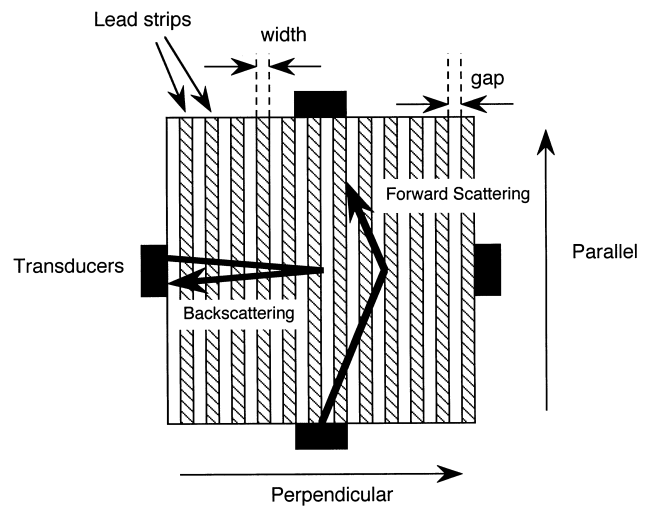
Shear (S) wave and compressional (P) wave piezoelectric transducers were used to send and receive waves propagated along the synthetic fracture. Two polarizations of the S-wave were used, one with the transverse particle motion oriented perpendicular to the interface (S_v) and the other transverse particle motion parallel to the interface (S_h). The P-wave has longitudinal particle motion oriented parallel to the direction of propagation along the interface. The transducers with a central frequency of 1 MHz were coupled with honey, held in place with a frame, and were mounted straddling the interface. The input pulse to the transducers consisted of a 250 V square pulse with a 0.4 μ s duration and a repetition rate of 100 Hz. The received waveforms were digitized and stored on a computer for analysis.

A synthetic fracture was created from two aluminum blocks (each 0.29 × 0.29 × 0.29 m) separated by asperities made of lead foil 25 microns in thickness. Several experiments were performed using different asperity widths and asperity spacings but with a constant asperity length of 0.29 m. The width of the asperities and the gap between the asperities used in the investigation are listed in Table 1 and a sketch of the distribution is shown in Fig. 1. Seismic wave measurements were also made on intact aluminum, away from the interface, for comparison with the seismic waveforms from the synthetic fracture. A normal load of 100,000 lbs was used to compress the asperities made from the lead foil.

4. Seismic waveforms

Fig. 2a shows the normalized received waveforms for S_v waves propagated parallel to the asperities and Fig. 2b shows the normalized received waveforms for

S_v waves propagated perpendicular to the asperities along the synthetic fractures with 1 × 1 mm, 2 × 2 mm, 4 × 4 mm, and 8 × 8 mm asperity periodicities (Table 1). Each data set also includes the propagated waveform through the bulk sample. The bulk S-wave is observed to arrive at 96 μ s in the signals recorded for the intact sample, as well as for all of the synthetic fractures. However, for the synthetic fractures most of the energy is partitioned into interface wave or Rayleigh model. For synthetic fractures 1 × 1 and 2 × 2, the



$$\text{Resonant (Bragg) Scattering Condition: } \sin \theta = \frac{\lambda}{2d}$$

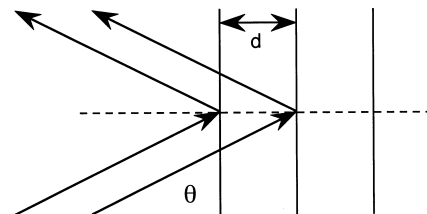


Fig. 1. Experimental arrangement of the synthetic fractures with lead strips and the piezoelectric transducers. Transmission perpendicular to the asperities produces resonant backscatter when the wavelength satisfies the Bragg condition. Transmission parallel to the asperities can lead to forward scattering.

arrival of an interface wave is observed around 100 μ s and is observed to contain low frequency components. For the 4×4 synthetic fracture when the asperity spacing is greater than the wavelength of the signal (3.4 mm) through the intact aluminum, a low-frequency interface wave is observed to carry some high frequency components which are associated with the propagation of a Rayleigh wave. For an asperity size and gap of 8 mm (8×8 synthetic fracture) the signal is composed of higher frequency components than those observed in the 1×1 and 2×2 synthetic fractures. The high frequency components are associated with Rayleigh waves. The evolution of the interface wave from the displacement discontinuity limit to Rayleigh limit can be seen clearly in this data, but a better decomposition in time and frequency is obtained using wavelet analysis in the next section.

An important contrast to the S_v -wave is the S_h -wave data shown in Fig. 3a and 3b for waveforms received parallel and perpendicular to the asperities, respectively. The S_h wave is not partitioned into an interface wave, and virtually all the waveforms are identical,

with only minor trends as the asperity size and gap go from 1 mm to 8 mm. The propagation is also virtually isotropic because this polarization is insensitive to the surface properties when propagating along the interface.

The received waveforms for P-waves propagated parallel and perpendicular to the asperities are shown in Fig. 4a and 4b, respectively. In sharp contrast to the case of the S_h waves, the P-wave is highly sensitive to the fracture asperity spacing, showing a clear evolution of behavior as the asperity size and gap increases from 1 mm to 8 mm. On the other hand, the waveforms are nearly isotropic with respect to the asperity orientation relative to the propagation direction.

5. Nolte–Hilbert wavelet

All time-varying signals can be viewed as combinations of waveforms that are localized in time and

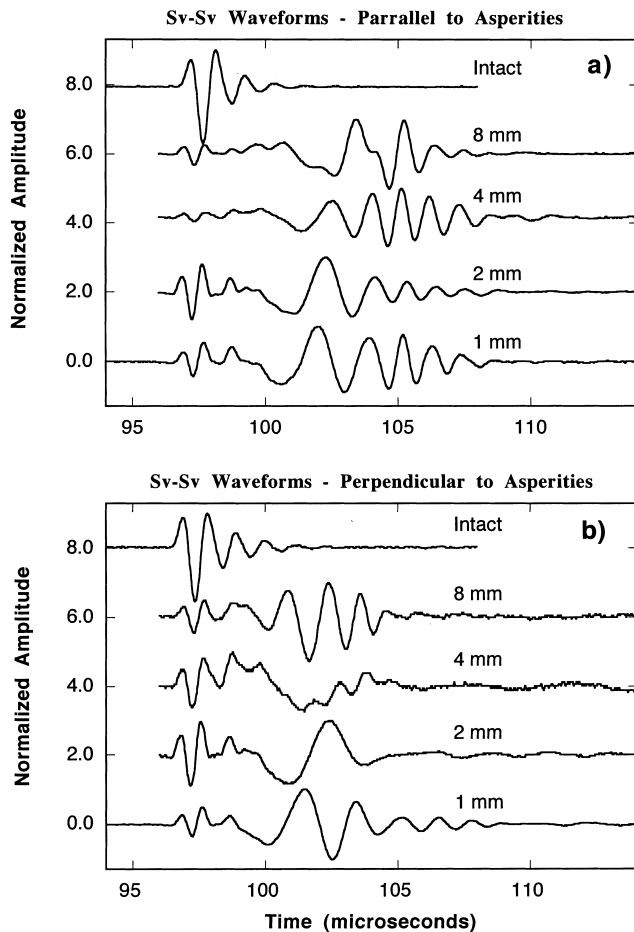


Fig. 2. S_v waveforms for propagation parallel (a) and perpendicular (b) to the asperities for increasing asperity size.

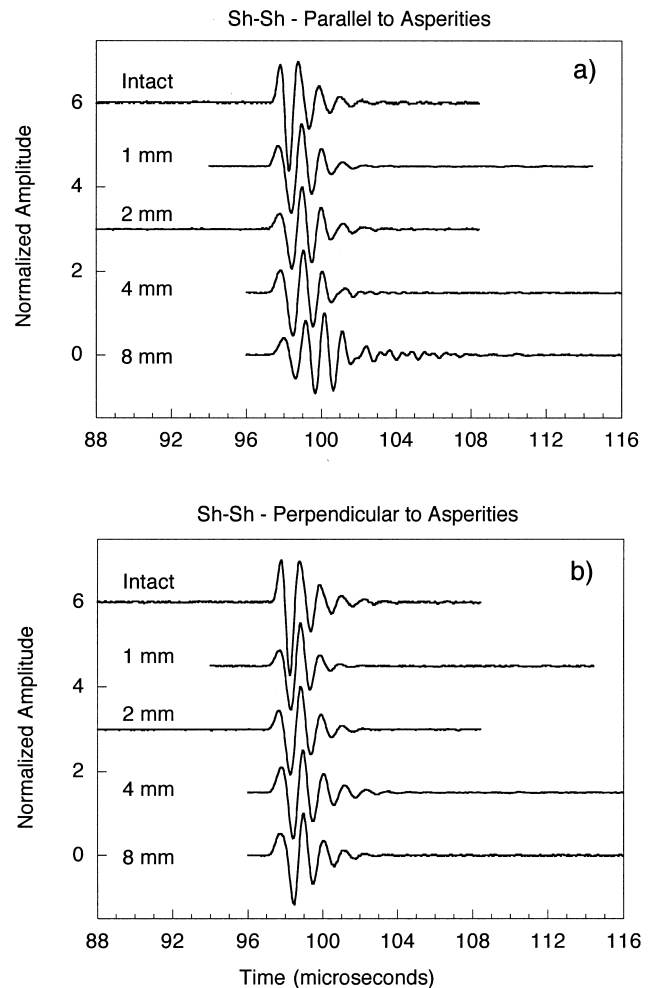


Fig. 3. S_h waveforms for propagation parallel (a) and perpendicular (b) to the asperities for increasing asperity size.

frequency. Each frequency component carries dynamic information about the system under study, while each time component carries kinetic information. Together, they contain the information necessary to extract dispersive properties, as well as the ability to identify distinctly different eigenmodes that co-propagate. The challenge is to find an optimal decomposition into time-frequency space to allow the best understanding of the physical processes under study.

Wavelet analysis is recognized as an important method for time-frequency decomposition. It is one of several windowed Fourier analysis techniques, but has the particularly attractive property that it maintains a constant time-bandwidth product as it is scaled through different frequencies. Maintaining the constant time-bandwidth product is important for applications such as the dispersion analysis of waves, because it inversely weights time and frequency in accordance

with the time-bandwidth product of transform-limited pulses.

Despite the value of maintaining a constant time-bandwidth product, wavelet analysis retains an ambiguity in the selective weighting in favor of either time localization or frequency localization. For some applications, frequency information is more important than time information, while the opposite can be true. These specific applications may then require the use of different wavelets. In the case of wave dispersion, it is important to give time-localization and frequency-localization equal weighting. This aspect was first pointed out by Pyrak-Nolte and Nolte [21], who used a Morlet wavelet [3,13] with a specific bandwidth that gave equal weighting to both time and frequency to extract the dispersion of a Rayleigh-mode interface wave.

The Morlet wavelet used in Pyrak-Nolte and Nolte [21] achieved the desired balanced weighting at the expense of the wavelet admissibility condition. The admissibility condition for a wavelet kernel is the requirement that the wavelet has a vanishing zeroth-order moment for all choice of wavelet scales. It is well known that the Morlet wavelet is never rigorously admissible as a wavelet kernel for a wavelet transform, and is only practically admissible for a large number of oscillations in the kernel. The oscillations allow the zeroth-order moment of the wavelet to integrate to values arbitrarily close to zero for increasing numbers of oscillations. The practical criterion for the Morlet wavelet is $\omega_0 > 5$, where the Morlet wavelet is given by

$$\psi = \pi^{-1/4} \exp\left(\frac{x^2}{2}\right) \exp(i\omega_0 x) \quad (1)$$

When the number of oscillations falls below this criterion, there is an increasing zeroth-order moment in the real part of the kernel that violates the admissibility condition and produces a spurious low-frequency response in the wavelet transform. However, the criterion $\omega_0 > 5$ is incompatible with the need for balanced time-frequency localization for dispersion analysis of short seismic pulses.

To resolve this incompatibility, we have developed a new wavelet kernel that explicitly balances time-frequency localization for short pulses, while rigorously satisfying the wavelet admissibility condition. This is achieved by first selecting only the imaginary part of the Morlet wavelet, which does by itself satisfy the admissibility condition, and then operating on it with a Hilbert transform to construct an orthogonal real-valued wavelet that also automatically satisfies the admissibility condition. The new complex wavelet is given by

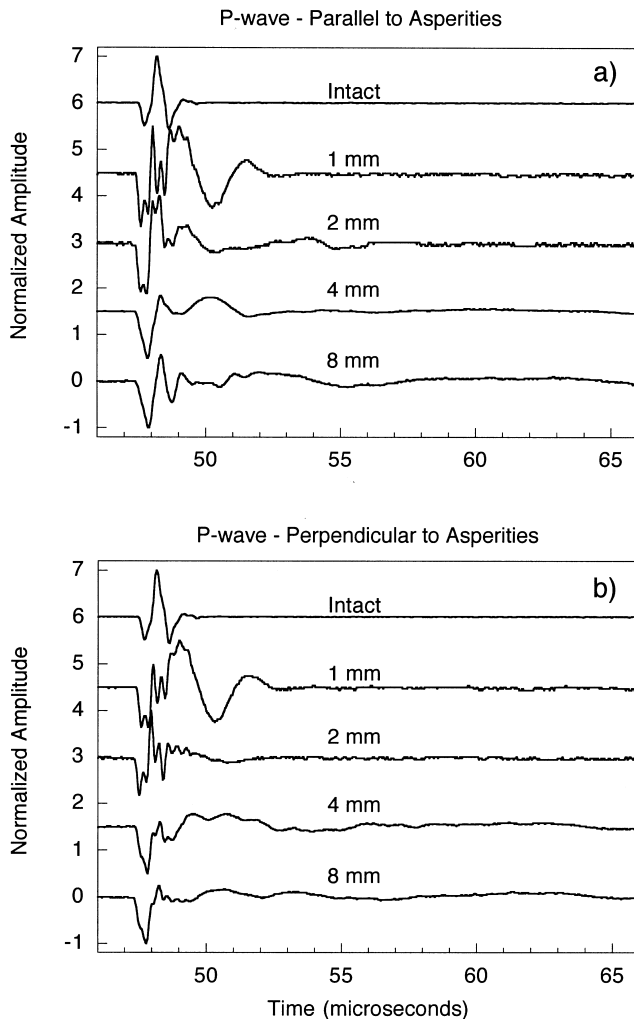


Fig. 4. P-waveforms for propagation parallel (a) and perpendicular (b) to the asperities for increasing asperity size.

$$\psi = \phi_1 + i\phi_2 \quad (2)$$

where

$$\phi_2 = \pi^{-1/4} \exp\left(-\frac{x^2}{2}\right) \sin(\omega_0 x) \quad (3)$$

and

$$\phi_1 = \mathcal{P} \int_{-\infty}^{\infty} \frac{\phi_2(u)}{x-u} du \quad (4)$$

where Eq. (4) defines the Hilbert transform. In practice, the integral in Eq. (4) is not performed numerically, because the divergent part can cause computational difficulties. Instead, the Hilbert transform is carried out in Fourier space, where it consists simply of changing the sign of half of the Fourier components of the function $\phi_2(\omega)$, and performing the inverse transform back into the time domain.

The Hilbert wavelet has many attractive features, with important properties. In the limit of large ω_0 , it goes continuously to the traditional Morlet wavelet with optimum frequency localization. In the limit of small ω_0 , it goes continuously to the complex combination of two well-known wavelets known as 1-DOG and 2-DOG (first-derivative of Gaussian and second-derivative of Gaussian) with optimum time localization. Most importantly for our applications, with the choice of $\omega_0 = \sqrt{2\pi}$ it provides the balanced time-frequency localization that is necessary for dispersion analysis of short pulses [21]. We will refer to this specific balanced wavelet as the Nolte–Hilbert wavelet to differentiate it from the general Morlet and DOG wavelets. The real and imaginary parts of the Nolte–Hilbert wavelet used in all subsequent wavelet analyses are shown in Fig. 5.

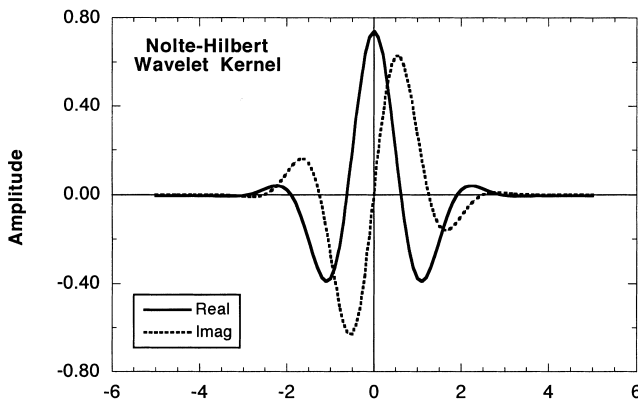


Fig. 5. Nolte–Hilbert wavelet kernel with balanced time and frequency localization using $\omega_0 = \sqrt{2\pi}$ in Eq. (3). The real and imaginary parts of the complex wavelet are shown individually. The integral of each component is rigorously zero, satisfying the wavelet admissibility condition.

6. Wavelet analysis

To quantify the frequency components of the signals, the Nolte–Hilbert wavelet was applied to the time-domain signals of Figs. 2–4 to obtain the time-frequency information from the received signals. In Fig. 6a and 6b, the wavelet transforms for synthetic fractures 1×1 , 2×2 , 4×4 , and 8×8 are shown for S_v waves propagating parallel and perpendicular, respectively, to the lead strips that define the fracture asperities. All of the wavelet transforms from the synthetic fracture show a faint energy (blue) at an arrival time of $97 \mu\text{s}$ which is the bulk shear wave with a dominant frequency of 0.92 MHz (with a wavelength of 3.4 mm).

The bulk shear wave is non-dispersive, as shown by the horizontal shape of this component of the wavelet transform. For the 1×1 and 2×2 synthetic fracture, most of the energy is partitioned into a dispersive interface wave with a dominant frequency of around 0.4 MHz (or wavelength of 7.7 mm). For the 4×4 synthetic fracture, when the asperity spacing is greater than a wavelength, the emergence of a non-dispersive Rayleigh is observed to occur at an arrival time of $105 \mu\text{s}$ in the case of propagation parallel to the strips, but the Rayleigh mode is virtually absent in the case of propagation perpendicular to the strips. The Rayleigh wave in the parallel case was observed as the high frequency components carried on the low frequency signal in Fig. 3.

Fig. 6b for propagation perpendicular to the asperities shows the existence of both a low-frequency interface wave arriving at $101 \mu\text{s}$ and a high-frequency Rayleigh wave at $105 \mu\text{s}$ for the 8×8 synthetic fracture. This coexistence of both modes results from the multi-component source, i.e. the low frequency components travel as interface waves and the high frequency components travel as Rayleigh waves. A striking feature is the gap that occurs in the spectrum between the low-frequency interface wave and the high-frequency Rayleigh wave. This gap is caused by the reflection of energy by the periodic asperity spacing.

Fig. 6 provides a striking contrast and comparison between the behavior of the S_v modes propagating parallel and perpendicular to the lead strips that define the fracture asperities. The most important difference is highlighted by comparing the parallel and perpendicular propagation conditions for the 4×4 fracture. In the case of parallel propagation (Fig. 6a), there is a clean dispersive trend that exhibits fast velocities of the interface wave at low frequency, going continuously over to the slower Rayleigh velocity at high frequencies. Forward scattering by the asperities is mostly absent, as evidenced by the lack of strong signals at later arrival times. However, in the case of perpendicu-

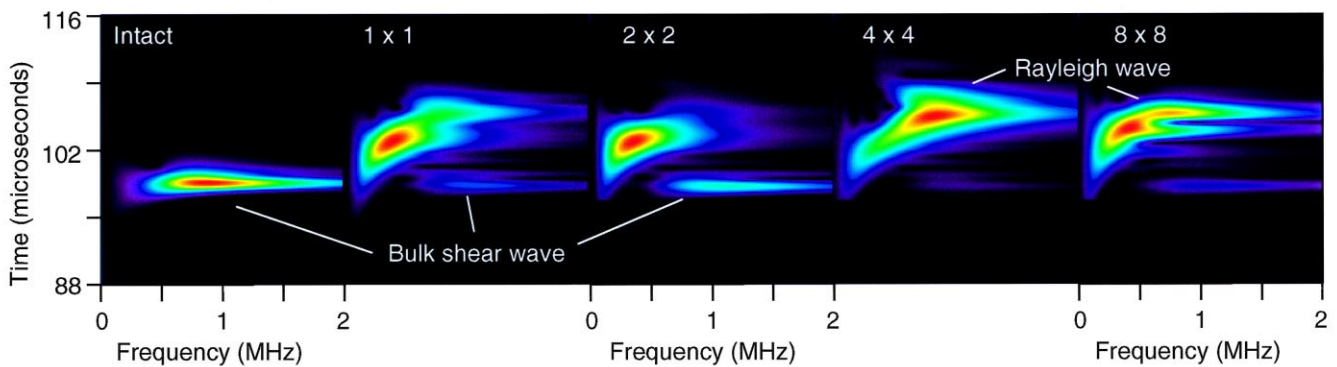
lar propagation (Fig. 6b) there is a dramatic absence of energy in the Rayleigh wave. Furthermore, the frequency spectrum of the interface wave is compressed towards low frequency in this case. These observations lead to clear trends as they are traced up to the 8×8 fracture and down to the 2×2 fracture. There is a clear compression of the interface-wave energy to lower frequency with increasing asperity separation, until the case of the 8×8 fracture, when nearly all the energy reemerges in the high-frequency Rayleigh mode, and the interface-wave mode has relatively little surviving energy.

The behavior of the perpendicular propagation case can clearly be interpreted in terms of resonant scattering and the formation of a stop-band in the transmission spectrum. The waves in this case are propagating across the asperities, which are placed in a periodic arrangement. When the asperity spacing is equal to $\lambda/2$, there is resonant reflection (Bragg reflection) of the seismic energy, leading to the formation of a notch, or stop band, in the transmitted spectrum. As the asperity size and gap goes from 2 mm, to 4 mm, to

8 mm, the stop-band frequencies are 0.73 MHz, 0.42 MHz, and 0.24 MHz, respectively. This sequence is inversely proportional to the asperity spacing. The decrease in the stop-band frequency for increasing asperity spacing is clearly seen in the wavelet transforms in Fig. 6b in the case of perpendicular propagation.

When the waves propagate parallel to the lead strips, there is also a possibility for resonant scattering in the forward direction through Bragg-reflection at glancing angles off the periodic asperities. This forward scattering would appear as late-arriving energy with the delay increasing with increasing frequency as the condition for Bragg reflection moves to higher scattering angles. The absence of such clear forward scattered energy may be caused by two possibilities. First, the lobe pattern of the transducers launches little energy at the higher angles that would be Bragg-matched. Second, the expected frequency dependence is very similar to the dispersion of the interface waves. Therefore in the case of propagation parallel to the asperities the situation may go smoothly from the interface wave

(a) Sv-wave: Parallel to Asperities



(b) Sv-wave: Perpendicular to Asperities

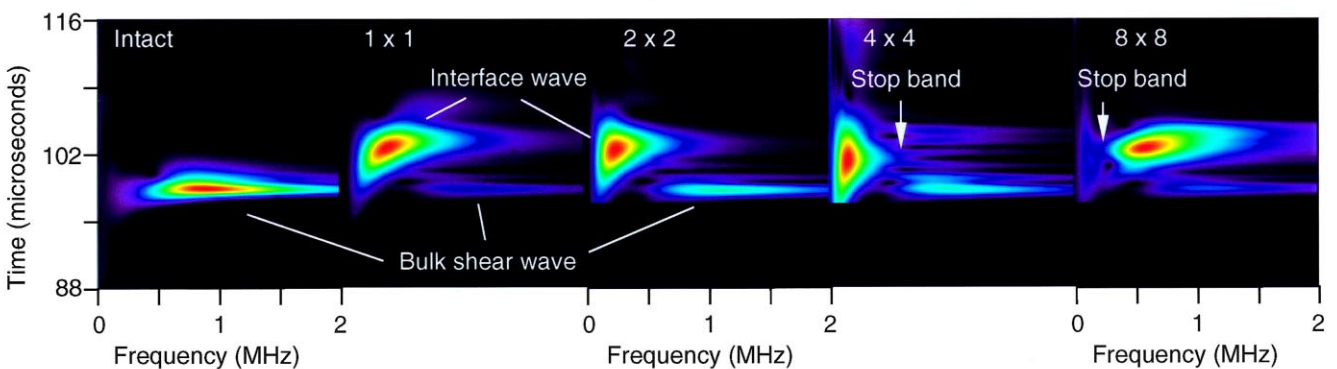


Fig. 6. Wavelet transforms of the S_v signals of Fig. 2, showing the intact 1×1 , 2×2 , 4×4 , and 8×8 transforms for waves propagating parallel (a) and perpendicular (b) to the asperities.

(displacement discontinuity) limit at low-frequency to forward scattering of Rayleigh waves at high frequency, without a clear demarcation between these two physically different situations.

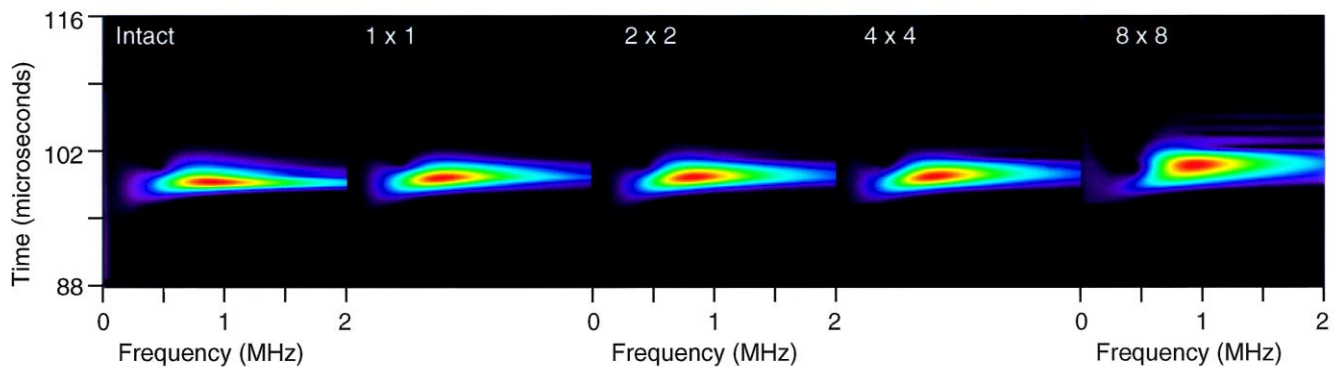
The interesting feature of the stop-band in the case of perpendicular propagation is that it provides a clear demarcation between interface wave propagation (in the displacement discontinuity limit) for frequencies below the stop-band, and the Rayleigh wave propagation for frequencies above the stop-band. Therefore, the ability to engineer the asperity spacing, combined with the broad-band frequency of the ultrasound pulse, provides a complete picture of the transition from the displacement discontinuity limit to the limit of resonant Rayleigh scattering by surface asperities.

It is important, next, to consider the control experiment presented by the S_h waves. This polarization has no associated interface wave, and all of the wavelet transforms, shown in Fig. 7, are practically identical for all asperity spacings and both propagation directions. One possible exception is the case of the 8×8 fracture for parallel propagation. Clear echoes are

observed in Fig. 7a for the 8×8 fracture that may be evidence for forward scattering, although the scattering of the S_h modes by the asperities is expected to be weak. Further attention to this feature would be necessary to resolve the issue.

The wavelet transforms for the P-mode signals are shown in Fig. 8. These transforms show distinctly different features than the S_h transforms. The most striking feature is the presence of an interference null in each of the fractured cases. An interference null occurs when there is exact destructive interference for a specific frequency and time. Such interference nulls occur in wavelet transforms when two distinct wave modes coexist and interfere, with the null occurring when the modes have opposite phases. In the earlier experimental work on P-interface-waves [25], these nodes were taken as direct evidence for a distinct interface wave that was not associated with the co-propagating bulk P-wave. A possible counter-explanation of the null was that the P-waves in the upper and lower half-spaces traveled at slightly different frequencies, leading to interference effects at the receiver. The com-

(a) S_h -wave: Parallel to Asperities



(b) S_h -wave: Perpendicular to Asperities

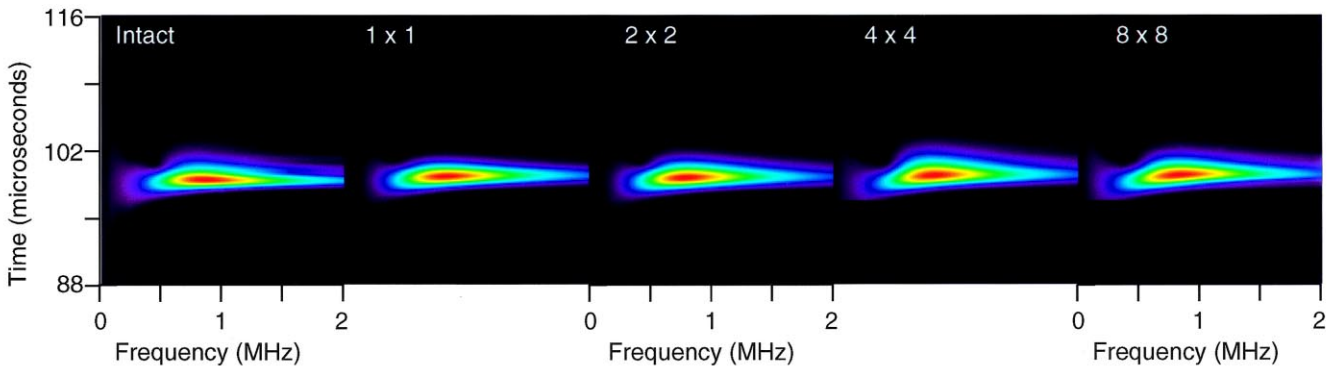


Fig. 7. Wavelet transforms of the S_h signals of Fig. 3, showing the intact 1×1 , 2×2 , 4×4 , and 8×8 transforms for waves propagating parallel (a) and perpendicular (b) to the asperities.

plete absence of such a null in the S_h transforms of Fig. 7 discounts this possibility here. Therefore, the interference null in the P-wave transforms provides further evidence for the presence of this distinct P-interface wave. The energy on the high-frequency side of the null is the bulk P-wave, while the energy on the low-frequency side of the null is the P-interface wave. This P-interface wave shows the opposite dispersion to the Rayleigh-mode interface wave, with slower velocities at lower frequencies.

A surprising aspect of the transforms shown in Fig. 8 is the nearly isotropic behavior of the P-mode interface wave, despite the strongly anisotropic asperity distribution. For instance, there is no clear evidence for a stop-band, as there was in the case of the S_v wave propagating perpendicular to the asperities. On the other hand, the frequency of the interference null does seem to depend on the asperity spacing, shifting to lower frequency as the spacing becomes wider. This movement of the null had been seen previously [15,25] as a function of fracture specific stiffness, with lower frequencies associated with lower stiffnesses. The absence

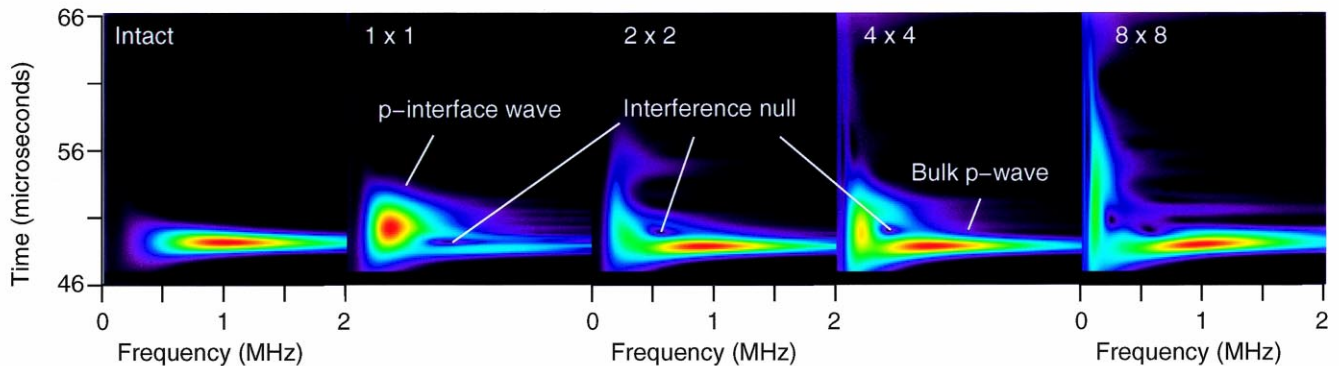
of anisotropy, however, remains an issue open to further research.

7. Interface-wave dispersion

The use of the time-frequency balanced Nolte–Hilbert wavelet makes it optimally suited to extract wave dispersion. This analysis was performed on each of the wavelets of Figs. 6–8. The results are shown in Figs. 9–11. For the S_v waves, the dispersion shows the traditional frequency-dependent signature of the Rayleigh-mode interface wave [17,21], with higher velocities at low frequencies trending towards the Rayleigh velocity at high frequencies. For both propagation directions, the wave dispersion is relatively insensitive to the asperity spacing. It is important to point out that in all these samples the contact area is constant. Therefore the stiffness may be approximately equal from the 1×1 sample up to the 8×8 sample, leading to nearly identical wave dispersions.

The dispersion observed in the S_h waves is caused

(a) P-wave: Parallel to Asperities



(b) P-wave: Perpendicular to Asperities

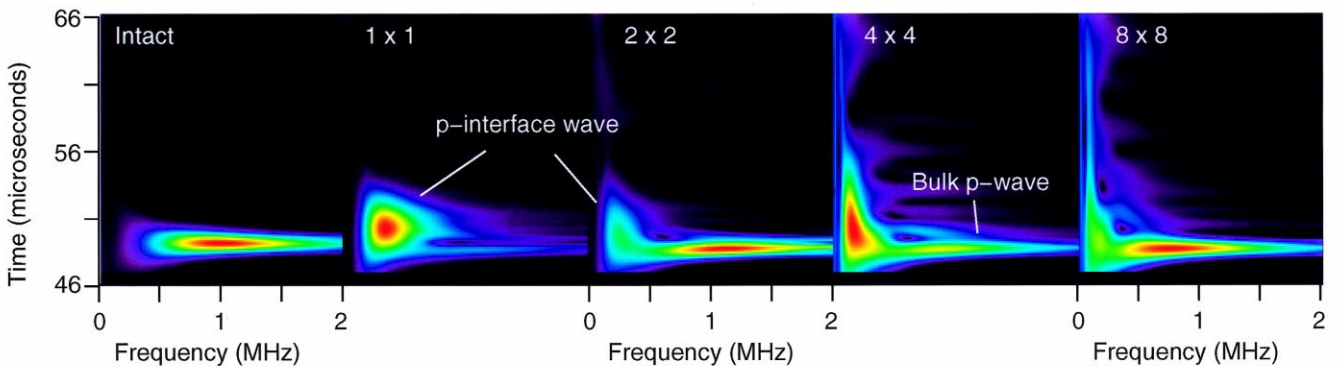


Fig. 8. Wavelet transforms of the P signals of Fig. 4, showing the intact 1×1 , 2×2 , 4×4 , and 8×8 transforms for waves propagating parallel (a) and perpendicular (b) to the asperities.

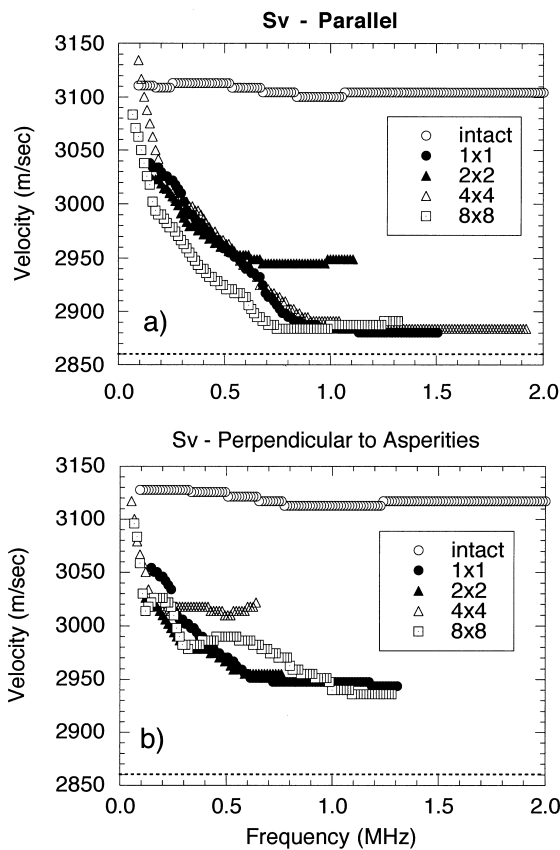


Fig. 9. Wave velocity dispersion extracted from the wavelet analysis of Fig. 6 for S_v wave propagation parallel (a) and perpendicular (b) to the asperities.

primarily by the system response, which can produce slightly chirped pulses. However, even in the case of the S_h waves, there is a slight increase in the chirp for the fractured cases relative to the intact cases. This may suggest a weak coupling of the S_h waves to the asperities, which may also explain the echoes seen in the case of S_h waves propagating in the 8×8 sample parallel to the asperities. Finally, in the case of the P-waves, the dispersion shows the opposite trend to the Rayleigh-mode interface waves. The lowest velocities occur at low frequencies, and trend towards the bulk P velocity at high frequencies.

8. Summary and conclusions

In this paper, we have specifically tracked the evolution of the seismic wave behavior as a function of asperity spacing for waves of all polarizations propagating along the interface. Several clear signatures were observed that help distinguish between the long-wavelength limit, in which the displacement discontinuity model is valid, and the short-wavelength limit, which is characterized by scattered Rayleigh waves.

In the case of S_v waves propagating perpendicular to the asperities, a clear stop-band caused by resonant back-scattering is observed that tracks with the increasing asperity spacing. This stop band provides a clear demarcation between the displacement discontinuity limit and the scattering regime. On the other hand, clear demarcation between these two regimes is apparent for the case of S_v waves propagating parallel to the asperities. The transition in this case is smooth, and the apparent dispersion observed in the 8×8 sample may be caused by forward scattering of Rayleigh waves, while the dispersion in the 1×1 sample can be clearly attributed to the fracture-interface wave.

The surprise in the case of the P-interface waves is the near isotropy of the wavelet spectra, despite the sensitivity of the P-wave to the asperity spacing. The low-frequency P-interface wave shows dispersion clearly opposite to the Rayleigh-mode interface wave with an interference null that clearly distinguishes it from the co-propagating bulk P-wave. It is possible that the isotropy is caused by the very low frequencies

of the P-interface wave. The low-frequency P-interface wave shows dispersion clearly opposite to the Rayleigh-mode interface wave with an interference null that clearly distinguishes it from the co-propagating bulk P-wave. It is possible that the isotropy is caused by the very low frequencies

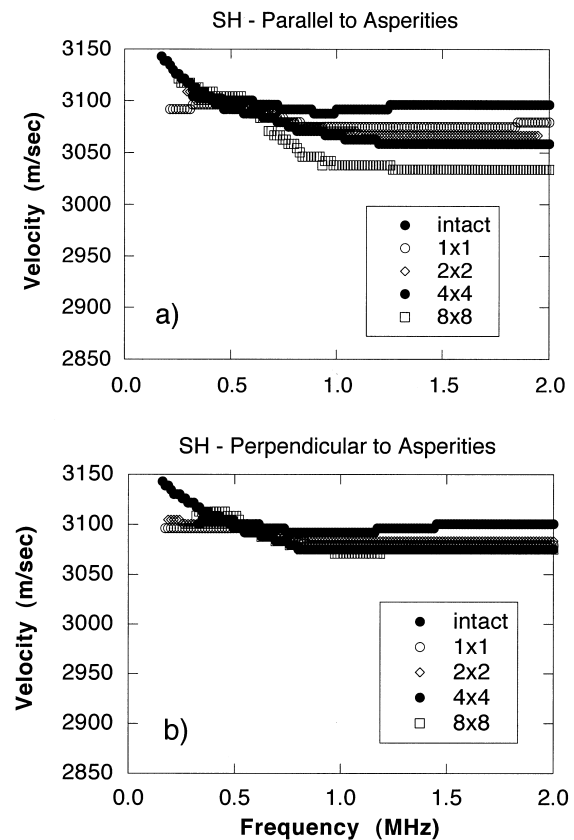


Fig. 10. Wave velocity dispersion extracted from the wavelet analysis of Fig. 7 for S_h wave propagation parallel (a) and perpendicular (b) to the asperities.

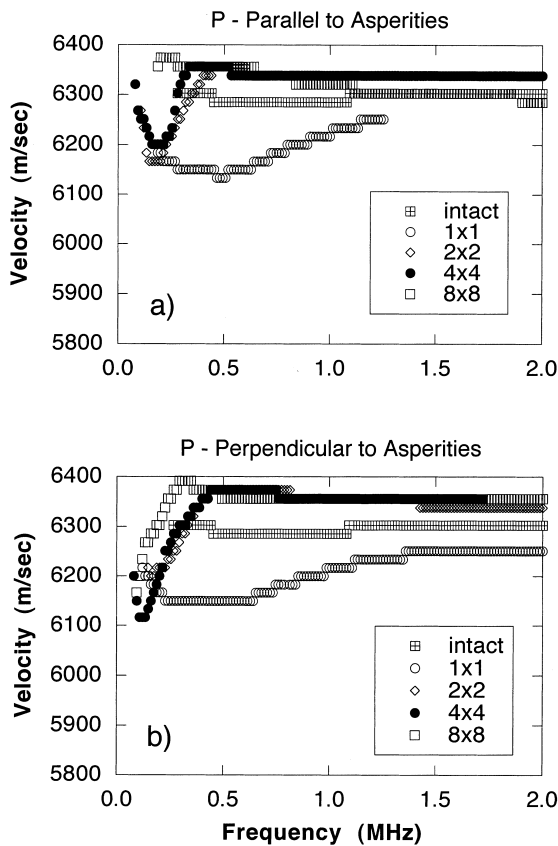


Fig. 11. Wave velocity dispersion extracted from the wavelet analysis of Fig. 8 for P-wave propagation parallel (a) and perpendicular (b) to the asperities.

and hence long wavelengths of the P-interface wave that places it firmly in the displacement discontinuity limit. However, this point remains an interesting question that is open to further research.

In conclusion, we have observed the transition from the displacement discontinuity limit into the Rayleigh-wave scattering regime. This transition can be a smooth transition in some cases, but may also be accompanied by a clear dividing line in the case of strong resonant back-scattering. The stiffnesses of all of the synthetic fractures appear to be relatively equal, leading to nearly identical wave dispersion in the displacement discontinuity limit. From these results, the displacement discontinuity theory is seen to remain robust, as is the concept of specific fracture stiffness, right up to the resonant scattering regime.

Acknowledgements

The authors wish to acknowledge support of this research by Department of Energy — Office of Basic

Energy Science (DE-FG02-97ER14785) and the Nation Science Foundation — Young Investigator Award (9896057).

References

- [1] Brown SR, Scholz CH. Closure of random surfaces in contact. *J Geophys Res* 1985;90:5531.
- [2] Brown SR, Scholz CH. Closure of rock joints. *J Geophys Res* 1986;91:4939.
- [3] Combes JM, Grossman A, Tchamitchian Ph, editors. *Wavelets: time–frequency methods and phase space*. Berlin: Springer-Verlag, 1989.
- [4] Cook NGW. Natural joints in rock: mechanical, hydraulic, and seismic behavior and properties under normal stress. *Int J Rock Mech Min Sci & Geomech Abstr* 1992;29:198–223.
- [5] Ekern A, Suarez-Rivera R, Hansen A. Investigation of interface wave propagation along planar fractures in sedimentary rocks. In: *Proceedings of the 35th US Symposium on Rock Mechanics*, 1995.
- [6] Fan J, Gu B, Nihei KT, Cook NGW, Myer LR. Experimental and numerical investigation of fracture interface waves. *Rock Mechanics Tools and Techniques*. In: *Proceedings of the 2nd North American Rock Mechanics Symposium*, Montreal, Quebec, Canada, 19–21 June, 1996. vol. 1. p. 845–51.
- [7] Greenwood JA, Williamson JBP. Contact of nominally flat surfaces. In: *Proceedings of the Royal Society, London, Ser. A* 295, 1966. p. 300–19.
- [8] Gu B. Interface waves on a fracture in rock, PhD Thesis, University of California, Berkeley, 1994.
- [9] Gu B, Nihei K, Myer LR, Pyrak-Nolte LJ. Interface waves. *Journal of Geophysical Research* 1995;101(1):827.
- [10] Hopkins DL, Cook NGW, Myer LR. Fracture stiffness and aperture as a function of applied stress and contact geometry. *Rock Mechanics*. In: *Proceedings of the 28th US Symposium*, 1987. p. 673–80.
- [11] Hopkins DL, Cook NGW, Myer LR. Normal joint stiffness as a function of spatial geometry and surface roughness. In: *International Symposium on Rock Joints*, 1990. p. 203–10.
- [12] Kitsunozaki C. Behavior of plane waves across a plane crack. *J Mining Coll Akita Univ* 1983;A3(6):173–87.
- [13] Morlet J, Arens G, Fargeau E, Giard D. Wave propagation and sampling theory — Part II: Sampling theory and complex waves. *Geophysics* 1982;47(2):222–36.
- [14] Nagy PB, Adler L. A novel technique for interface wave generation. In: Leroy O, Breazeale MA, editors. *Physical acoustics*. New York: Plenum Press, 1991.
- [15] Nolte DD, Pyrak-Nolte LJ. Quantifying Fracture Evolution through Wavelet Analysis. In: *Fall Meeting of the American Geophysical Union*, 8–12 December 1997, San Francisco, CA, 1997. vol. 78. p. F33.
- [16] Pyrak-Nolte LJ, Myer LR, Cook NGW. Transmission of seismic waves across natural fractures. *Journal of Geophysical Research* 1990;95(B6):8617–38.
- [17] Pyrak-Nolte LJ, Cook NGW. Elastic interface waves along a fracture. *Geophysical Research Letters* 1987;14(11):1107–10.
- [18] Pyrak-Nolte LJ, Myer LR, Cook NGW. 1987. Seismic visibility of fractures. *Rock Mechanics*. In: Farmer IW, Daemen JJK, Desai CS, Glass CE, Neuman SP, editors. *Proceedings of the 28th US Symposium*, University of Arizona, Tucson, June. Boston: AA Balkema, 1987. p. 47–56.
- [19] Pyrak-Nolte LJ, Nolte DD. Frequency dependence of fracture stiffness. *Geophys Res Lett* 1992;3(19):325–8.
- [20] Pyrak-Nolte LJ, Xu J, Haley GM. Elastic interface waves pro-

- pagating in a fracture. *Physical Review Letters* 1992;68(24):3650–3.
- [21] Pyrak-Nolte LJ, Nolte DD. Wavelet analysis of velocity dispersion of interface waves along fractures. *Geophysical Research Letters* 1995;22(11):1329.
- [22] Pyrak-Nolte LJ, Morris JP. Single fractures under normal stress: The relation between fracture specific stiffness and fluid flow, submitted to this special issue of the *International Journal of Rock Mechanics Mining Science & Geomechanics Abstracts*, 2000;37(1):245–262.
- [23] Rokhlin SI, Wang YJ. Analysis of boundary conditions for elastic wave interaction with an interface between two solids. *J Acoustic Soc Am* 1991;65(8):503–15.
- [24] Roy S, Pyrak-Nolte LJ. Interface waves propagating along tensile fractures in dolomite. *Geophys Res Lett* 1995;22(20):2773–7.
- [25] Roy S, Pyrak-Nolte LJ. Observation of a distinct compressional-mode interface wave on a single fracture. *Geophys Res Lett* 1997;24(2):173–6.
- [26] Schoenberg M. Elastic wave behavior across linear slip interfaces. *J Acoust Soc Am* 1980;5(68):1516–21.
- [27] Pyrak-Nolte LJ, Shiau J-Y. Compressional wave anisotropy caused by single and multiple fractures. *SPE/ISRM Eurock '98*, Trondheim, Norway, 8–10 July 1998, SPE 47366.
- [28] Pyrak-Nolte LJ, Mullenbach BL, Roy S. Interface waves along fractures. *J Appl Geophys* 1996;35:79–87.